From crater functions to partial differential equations: a new approach to ion bombardment induced nonequilibrium pattern formation

2009 J. Phys.: Condens. Matter 21 224017

(http://iopscience.iop.org/0953-8984/21/22/224017)

J. Phys.: Condens. Matter **21** (2009) 224017 (11pp) doi:10.1088/0953-8984/21/22/224017

From crater functions to partial differential equations: a new approach to ion bombardment induced nonequilibrium pattern formation

Scott A Norris, Michael P Brenner and Michael J Aziz

Harvard School of Engineering and Applied Sciences, Cambridge MA 02138, USA

Received 11 February 2009
Published 12 May 2009
Online at stacks.iop.org/JPhysCM/21/224017

Abstract

We develop a methodology for deriving continuum partial differential equations for the evolution of large-scale surface morphology directly from molecular dynamics simulations of the craters formed from individual ion impacts. Our formalism relies on the separation between the length scale of ion impact and the characteristic scale of pattern formation, and expresses the surface evolution in terms of the moments of the crater function. We demonstrate that the formalism reproduces the classical Bradley–Harper results, as well as ballistic atomic drift, under the appropriate simplifying assumptions. Given an actual set of converged molecular dynamics moments and their derivatives with respect to the incidence angle, our approach can be applied directly to predict the presence and absence of surface morphological instabilities. This analysis represents the first work systematically connecting molecular dynamics simulations of ion bombardment to partial differential equations that govern topographic pattern-forming instabilities.

1. Introduction

Uniform ion beam sputter erosion of a solid surface often causes a spontaneously-arising pattern in the surface topography that can take the form of corrugations or arrays of dots [1, 2]. On the one hand, periodic self-organized patterns with characteristic spacing as small as 7 nm [3] have stimulated interest in this method as a means of sub-lithographic nanofabrication [4]. The apparent scaling of the characteristic spacing with ion energy [2] serves as an additional motivation for the thorough understanding of the low-energy regime. On the other hand, it is known empirically that the same ion beam on the same surface can cause pattern formation under some conditions (e.g. angle of incidence) and surface smoothing under other conditions. A fundamental understanding of the origins of roughening and smoothing could therefore have important implications for engineered surface smoothing [5] as well as simply avoiding roughening when too much of the latter is a problem, e.g. in focused or unfocused ion milling or sample preparation for cross-section transmission electron microscopy [6].

The ion sputtering process results from the nuclear collision cascade accompanying the ion impact. All existing theories of sputter morphology evolution originate from Sigmund's 1973 model demonstrating the instability of a planar surface to uniform ion beam erosion [7, 8]. According to Sigmund, in one spatial dimension, the (normal) rate of recession of an eroding surface v at a point $\mathbf{x}$ on the surface is proportional to the total energy deposited there from impacts at nearby points $\mathbf{x}'$. This can be expressed

$$v(\mathbf{x}) = \int E(\mathbf{x}, \mathbf{x}')\, \mathrm{d}\mathbf{x}', \tag{1}$$

where $E(\mathbf{x}, \mathbf{x}')$ is the energy reaching $\mathbf{x}$ from an impact at $\mathbf{x}'$. For simplicity, Sigmund modeled the distribution of deposited energy as centered a distance a below the impingement site (along the initial ion direction) and decaying outward as a Gaussian ellipsoid with standard deviations σ and μ in the longitudinal and transverse directions, respectively. Because ions penetrate the surface some distance before releasing their energy, most of the energy is released 'downbeam' of the impact point. Sigmund observed that this structure generically implied a roughening instability, because valleys, being

'downbeam' compared to hilltops, undergo more erosion. This observation was investigated in more detail by Bradley and Harper [9] (BH), who performed a linear stability analysis of a flat surface undergoing erosion from Gaussian ellipsoid collision cascades while simultaneously undergoing surface relaxation toward flatness by surface diffusion. By expanding the surface in a small curvature, they reduced Sigmund's non-local integral (1) to a series of local partial differential terms, including a destabilizing second-order term. The same expansion for the diffusional relaxation term is taken from the classical Mullins/Herring [10, 11] theory of morphological relaxation kinetics, yielding a fourth-order smoothing term. This important result showed that the instability survives no matter the amount of simultaneous relaxation, explained the selection of specific dominant wavelengths, and additionally predicted the oft-observed rotation of ripples from parallel-mode (wavevector parallel to projected ion beam direction) to perpendicular-mode (wavevector perpendicular to ion beam) at high angles from normal incidence.

While the Bradley–Harper theory successfully explained the qualitative aspects of ripple formation described above, it failed in a number of ways to quantitatively agree with experiments. These are by now well documented in the literature, and include such discrepancies as the existence of stable regimes; incorrect scaling of the wavelength with quantities such as flux, energy, and temperature; and incorrect prediction of the direction of ripple propagation. The reader is referred to [2] for a recent summary of the situation. So recent work in the field has been devoted to generalizing the BH model to bring it into better agreement with experiment. Broadly, the two main components of most sputter pattern formation models can be represented by re-writing the erosion velocity at a point $\mathbf{x}$ as

$$v(\mathbf{x}) = v_{\mathrm{P}}(\mathbf{x}) + v_{\mathrm{G}}(\mathbf{x}). \tag{2}$$

Here, on the one hand, $v_{\mathrm{P}}(\mathbf{x})$ models the short-time or *prompt regime*, concerned with local, single ion impacts occurring over picoseconds, and the coarse-grained cumulative effect of many individual ion impacts. For example, BH expand the Sigmund erosive integral to first order in a small curvature, while enhancements over the past decade include higher-order expansions of the same [12–14], revisions to Sigmund's ellipsoids [15, 16], or the inclusion of non-erosive elements [17–19]. On the other hand, $v_{\mathrm{G}}(\mathbf{x})$ models the long-time or *gradual regime*, which is concerned with global relaxation dynamics occurring over much longer times. Here, BH use Mullins surface diffusion, while more recent works introduce theories of ion-enhanced viscous flow [20, 21] or a damping term hypothesized to stand for an as-yet-unverified long-range redeposition mechanism [22, 23]. However, there is as yet no comprehensive combination of prompt- and gradual regime theories that is consistent with the full range of observed behaviors.

In this work we will concern ourselves almost exclusively with the prompt regime component $v_{\mathrm{P}}(\mathbf{x})$, where current interest focuses on isolating the 'crater function'—the function describing the average change in surface shape due to the impact of a single ion. Of particular interest is the study of atomic *redistribution*. For high ion energies and masses, it is well known that surface bombardment can lead to formation of craters with rims, which indicate a large number of atoms redistributed on the surface rather than sputtered. At low ion energies, although well-defined craters do not usually form, an 'average' cratering behavior with significant atom redistribution persists [24, 25]. Furthermore, with decreasing ion energy the relative importance of surface transport compared to bulk transport processes increases to the point where the former has major implications for pattern formation. Critically, this redistributive behavior has been largely neglected in analyses—although leading-order approximations of this effect exist [17, 18, 16], a comprehensive connection between microscopic impact responses and the macroscopic evolution equation is still missing[1]. Highlighting the importance of this point, recent theoretical studies [16] have shown that small changes in the shape of the crater function can lead to substantial changes in the behavior of the macroscopic system. This is well illustrated by early work on redistribution by Carter and Vishnyakov [17]. Using a model whereby off-normal ion incidence would cause a downbeam surface current of atoms along the surface, they showed that this *ballistic atomic drift* acts as a stabilizing force for near-normal incidences, by driving mass 'downhill' into valleys, and mitigating against preferential sputtering there. In appropriate parameter regimes, this effect can make flat surfaces stable at low angles, thus fundamentally altering the stability landscape!

Because of the sensitive dependence of macroscopic pattern-forming behavior upon the microscopic impact response, it is imperative (a) to obtain accurate knowledge of the erosive and (especially, due to their relative novelty) redistributive components of the crater function, and then (b) to rigorously connect these aspects of ion impact to the associated $v_{\mathrm{P}}(\mathbf{x})$ found in a continuum PDE. For the first half of this program, while results from physical experiments exist [27, 24], molecular dynamics (MD) simulations are increasingly being used [18, 15, 25]. The unanswered question that remains, then, is how to translate a known crater function into continuum equations capable of predicting macroscopic pattern-forming behavior. It is this question we address here. We write the surface evolution as a flux-weighted integral of the crater function [28, 16]:

$$v_{\mathrm{P}}(\mathbf{x}) = \int I(\mathbf{u}) g\left(\mathbf{u}; \nabla h, \nabla^2 h, \ldots\right) \mathrm{d}\mathbf{u} \tag{3}$$

where I is the flux, $\mathbf{u} = (u, v)$ is a co-ordinate plane tangent to the surface at $\mathbf{x}$, and the crater function $g = \Delta h$ is the *average* local change in topography for a single ion impact; it

[1] We note, however, a significant body of work that takes an alternate approach, treating redistribution in a phenomenological way by comparing it to the process of sand dune evolution [26, 19]. There, with the assumption of certain generic behaviors, equations are produced which, under numerical integration, can be parametrically tuned to mimic experimental images. However, in nature the system parameters are generally not tunable, but rather given, and one would like a theory which predicts system behavior based on the given parameters. Since these works are not explicitly connected to the microscopic picture, they are difficult or impossible to rigorously compare with experiments.

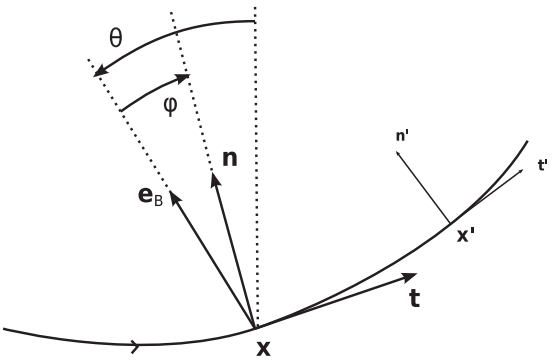

Figure 1. An illustration of the conventions used in the one-dimensional system, with local co-ordinates about a point $\mathbf{x}$ of primary interest, and also about a nearby point $\mathbf{x}'$. Here the vertical dotted line corresponds to 'up' in the global laboratory co-ordinates; thus θ is the experimental incidence angle, while ϕ is the local incidence angle.

is always expressed with respect to the local co-ordinate plane, and contains both the erosive and redistributive components of the surface response. We then perform a 'small curvature expansion' in a small parameter ε related to the ratio of impact to relaxation scales, to obtain at last a local PDE of the form

$$v_{\mathrm{P}} = \left(I\tilde{M}^{(0)}\right) + \varepsilon\nabla_{\mathbf{S}}\cdot\left(I\tilde{M}^{(1)}\right) + \tfrac{1}{2}\varepsilon^2\nabla_{\mathbf{S}}\cdot\nabla_{\mathbf{S}}\cdot\left(I\tilde{M}^{(2)}\right) + \cdots, \tag{4}$$

where $\nabla_{\mathbf{S}}$ represent surface divergences, and the tensors $\tilde{M}^{(i)}$ are obtained directly from the crater function. Crucially, these terms are simply combinations of the *moments* of the single ion response functions, which are obtainable directly via experiment or MD simulation. Thus, this work presents a unified framework that is grounded in—and directly incorporates—the response of the surface to single ion impacts.

2. Theory—one dimension

In this section we develop a continuum approach to sputtering that depends, ultimately, only on the moments of the responses to a single ion impact. Thus, it is a natural framework in which to incorporate the results of molecular dynamics simulations. Because of some subtleties in the theory, we first develop it thoroughly in one independent spatial dimension here, before generalizing to two independent spatial dimensions in section 3.

2.1. Preliminaries

In figure 1, we see a target surface being bombarded by ions at a lab frame incidence angle of θ, and we introduce a *fixed* vector $\mathbf{e}_{\mathrm{B}}$ that points at the irradiation source. At any particular point $\mathbf{x}$ on this surface, the tangent is given by $\mathbf{t}$, the normal by $\mathbf{n}$, and the *local* incidence angle—the angle between $\mathbf{e}_{\mathrm{B}}$ and $\mathbf{n}$—is written as ϕ and satisfies $\cos\phi = \mathbf{e}_{\mathrm{B}}\cdot\mathbf{n}$. Furthermore, we may construct about $\mathbf{x}$ a *local* co-ordinate system (u, w) associated, respectively, with the basis vectors $\mathbf{t}$ and $\mathbf{n}$. Thus, in the vicinity of $\mathbf{x}$, the surface can be described as $w = h(u)$, and surface points $\mathbf{x}'$ near $\mathbf{x}$ can be written

$$\mathbf{x}' = (u, h(u)). \tag{5}$$

Furthermore, we assume an *a priori* knowledge (whether from experiment, MD simulation, or otherwise) of the crater function describing the average surface response to a single ion impact. To describe the effect of an impact at the point $\mathbf{x}'$ (not necessarily related to $\mathbf{x}$), we write

$$\Delta h(u') = g\left(u'; \mathcal{S}(x')\right) \tag{6}$$

(note that the point $\mathbf{x}'$, being distinct from $\mathbf{x}$, possesses an associated distinct local co-ordinate system (u', w')—this will become important shortly). In this function the first argument u' refers to the u'-dependence of Δh, while the second argument $\mathcal{S}(x')$ denotes a parametric dependence of the function g on the geometry of the surface near $\mathbf{x}'$. In particular, g must depend at least on the local incidence angle $\phi(\mathbf{x}')$ for consistency with the sputter yield curve; it may also depend on higher derivatives such as curvature (we note, however, that in Sigmund's mechanism, g is independent of curvature: the curvature dependence of v_{P} there comes from integrating g over a curved surface).

2.2. Continuum erosion rate

Given the representation (6) describing the effect of a single ion impact at $\mathbf{x}'$, let us now construct a continuum model that gives the prompt contribution v_{P} to the erosion rate at $\mathbf{x}$ due to a flux of ions. Because the function g describes the surface response caused by impact from a single ion, we assume that the evolution at $\mathbf{x}$ due to a flux I of ions can be obtained by integrating the responses arising from many impacts at points $\mathbf{x}'$ near $\mathbf{x}$, multiplied by the strength of the flux at those points[2]. However, the process is complicated by the nature of g, which is only known in terms of the local co-ordinate system about the impact point. Thus, while our question on the erosion rate at $\mathbf{x}$ is most naturally posed in the (u, w) co-ordinates anchored there, the responses due to impacts at nearby points $\mathbf{x}'$ are most naturally expressed in the respective co-ordinates (u', w') centered on those points. Thus, a conversion between the two co-ordinate systems is required. To perform this conversion, we introduce a function

$$c(u) = \left(\mathbf{x} - \mathbf{x}'\right)\cdot\mathbf{t}' = -ut'_u(u) - h(u)t'_w(u), \tag{7}$$

which represents the lateral co-ordinate of the point $\mathbf{x}$ as seen from the nearby point $\mathbf{x}'$ (see figure 1), and where t'_u and t'_w are just the components of $\mathbf{t}'$. With this tool at our disposal, we can now easily write down the integrated behavior at $\mathbf{x}$ in the form[3]

$$v_{\mathrm{P}}(\mathbf{x}) = \int_{-\infty}^{\infty} R(u)\,\mathrm{d}u = \int_{-\infty}^{\infty} I(u)g\left(c(u); \mathcal{S}(u)\right)\,\mathrm{d}u \tag{8}$$

[2] Mathematically, this approach is essentially taking g to be the Green's function for the ion bombardment process. Physically, it implies an assumption that the surface has approximately uniform structure, allowing the neglect of variations due to local material history (e.g., poor bonding due to prior impacts).

[3] We note that there is a canceled factor of $\mathbf{n}\cdot\mathbf{n}'$ in equation (8): we multiply the integrand by this factor to account for the projection of the response at $\mathbf{x}'$ onto the normal $\mathbf{n}$, but then we divide to account for the length of the surface element at $\mathbf{x}'$.

(here $R(u) = I(u)g(u)$ is introduced purely for syntactical reasons). Finally, we note that under irradiation with a uniform-intensity ion beam, the projected ion flux $I(u)$ at the point $(u, h(u))$ depends only on the local incidence angle as

$$I(u) = I_0 \mathbf{e}_B \cdot \mathbf{n} = I_0 \cos\phi(u), \tag{9}$$

where I_0 is the flux through a plane perpendicular to $\mathbf{e}_B$, and $\cos\phi$ describes beam dilution due to off-normal incidence.

Before proceeding, we make a couple of comments about the quantity $c(u)$. First, we note that this construction is not present in existing theories based on Sigmund's model of erosion. This is because Sigmund's model posits an underlying physical picture of energy release that does not depend on surface shape—i.e., the model is *co-ordinate independent*. Here, in contrast, we have no underlying co-ordinate independent model, and the surface response is expressed in terms of the local co-ordinate system at the point of impact; it is this constraint that necessitates $c(u)$. Second, we note that if the surface is nearly flat (see below), then $h(u)$ and $t_w(u)$ are nearly zero, and hence as a first-order approximation $c(u) \approx -u$.

2.3. Multiple-scale analysis

The first key step in our argument is to make the common observation that the typical length scale of observed surface structures is much larger than the length scale of a typical ion impact—i.e., on the scale of the ion impact range, the surface shape $\mathcal{S}$ varies slowly. Because the integrand $R(u)$ depends both on the shape of the crater function, and also on the shape of the surrounding surface, it therefore contains two disparate length scales. To formally encode these notions, we introduce 'small' or 'slow' space variables (U, W) given by

$$\begin{bmatrix} U \\ W \end{bmatrix} = \varepsilon \begin{bmatrix} u \\ w \end{bmatrix}, \tag{10}$$

where ε is a small parameter taken to be the ratio of the average ion penetration depth to a length scale associated with macroscopic relaxation (see appendix A for more details). Thus, on the scale of the crater size (fast variable u), the surface shape varies slowly (slow variable U). We use these variables to express the integrand of (23) as

$$R(u) = \tilde{R}(u, U) = \tilde{I}(U) g\left(\tilde{c}(u, U); \tilde{\mathcal{S}}(U)\right). \tag{11}$$

While this looks complicated, here tildes simply indicate that (u, w) have been replaced by (U, W) where appropriate: i.e.

$$\begin{aligned} \tilde{I}(U) &= I(u) \\ \tilde{\mathcal{S}}(U) &= \mathcal{S}(u) \\ \tilde{c}(u, U) &= -(u, h(U)) \cdot \mathbf{t}'(U) = c(u). \end{aligned} \tag{12}$$

Together, the combination of variables u and U in equations (11) and (12) indicate that, on the scale of the impact range, the surface shape—and hence the height, tangent, normal, and flux—varies slowly in the vicinity of the point $\mathbf{x}$. This leaves the spatial dependence of the surface response as the only fast-varying quantity.

Our mathematical approach to exploiting this disparity in length scales is thus slightly more formal than that found in the literature to date. However, we do not employ this precision for its own sake, as we shall see. Because the function $\tilde{R}(u, U)$ depends on the small variable U, we now immediately Taylor expand $\tilde{R}$ in U, obtaining after some substitutions the equivalent expressions

$$\begin{aligned} \tilde{R}(u, U) &= [\tilde{R}]_{U=0} + U\left[\partial_U \tilde{R}\right]_{U=0} + \tfrac{1}{2}U^2\left[\partial_{UU}\tilde{R}\right]_{U=0} \\ &\quad + \cdots \\ R(u) &= [\tilde{R}]_{U=0} + \varepsilon u\left[\partial_U \tilde{R}\right]_{U=0} \\ &\quad + \tfrac{1}{2}(\varepsilon u)^2\left[\partial_{UU}\tilde{R}\right]_{U=0} + \cdots. \end{aligned} \tag{13}$$

2.4. Expression in terms of effective moments

We now come to the second key step of our argument. Inserting equation (13) into equation (8), we see that the (scalar) normal velocity $v_\mathbf{n}$ is obtained from the two-argument function $\tilde{R}(u, U)$ in three stages: first, one Taylor expands $\tilde{R}$ about $U = 0$; second, one performs the substitution $U \to \varepsilon u$; and last, one integrates in u. However, since u and U are formally independent variables, the ordering of the U-derivatives and u-integration can be reversed! So we alter the ordering of the operations by integrating first. Dispensing now with the notation R, we then obtain after some manipulation the following

$$\begin{aligned} v_P(\mathbf{x}) = I_0\Big[&\left(\tilde{M}^{(0)}\cos\phi\right) + \varepsilon\partial_U\left(\tilde{M}^{(1)}\cos\phi\right) \\ &+ \tfrac{1}{2}\varepsilon^2\partial_{UU}\left(\tilde{M}^{(2)}\cos\phi\right) + \cdots\Big]_{U=0}, \end{aligned} \tag{14}$$

where the *effective moments* $\tilde{M}^{(i)}$ are written in the form

$$\begin{aligned} \tilde{M}^{(0)}(U) &= \int g\left(\tilde{c}(u, U), U\right) \mathrm{d}u \\ \tilde{M}^{(1)}(U) &= \int g\left(\tilde{c}(u, U), U\right) u \,\mathrm{d}u \\ \tilde{M}^{(2)}(U) &= \int g\left(\tilde{c}(u, U), U\right) u^2 \,\mathrm{d}u \\ &\cdots. \end{aligned} \tag{15}$$

2.5. Conversion to actual moments

Equations (14) and (15) are the central result of this section. However, one small problem remains—the quantities $\tilde{M}^{(i)}$ are moments of the compound function $g(c(u))$; our stated goal was to seek an expression using the true moments $M^{(i)}$ of the

original crater function $g(u)$:

$$\begin{aligned} M^{(0)}(U) &= \int g\,(u;\ \mathcal{S}(U))\ \mathrm{d}u \\ M^{(1)}(U) &= \int g\,(u;\ \mathcal{S}(U))\,u\,\mathrm{d}u \\ M^{(2)}(U) &= \int g\,(u;\ \mathcal{S}(U))\,u^2\,\mathrm{d}u \\ &\ldots. \end{aligned} \tag{16}$$

So, to reach our final goal, we perform the change of variables

$$u \to c^{-1}(u, U) = -t_u(U)^{-1}\,[u + h(U)t_w(U)] \tag{17}$$

in the integrations (15). After some simple but tedious calculation, this allows us to write the effective moments $\tilde{M}^{(i)}$ in terms of the true moments $M^{(i)}$ via the relations

$$\begin{aligned} \tilde{M}^{(0)} &= -(-t_u)^{-1}\left[M^{(0)}\right] \\ \tilde{M}^{(1)} &= -(-t_u)^{-2}\left[M^{(1)} + (ht_w)\,M^{(0)}\right] \\ \tilde{M}^{(2)} &= -(-t_u)^{-3}\left[M^{(2)} + 2(ht_w)M^{(1)} + (ht_w)^2 M^{(0)}\right] \\ &\ldots, \end{aligned} \tag{18}$$

where the extra factor of $(-t_u)^{-1}$ comes from the result of the co-ordinate change on $\mathrm{d}u$, and the negative sign comes from the corresponding need to flip the integral.

2.6. Comments

As claimed in the introduction, equations (14) and (18) indicate that the surface dynamics of the prompt regime $v_{\mathrm{P}}(\mathbf{x})$ can be reduced to a local expansion involving only the (pure) moments of the crater function $g(u)$. This result yields several benefits worth summarizing. First, in this form, the connection with the prompt regime of ion impact is clear, and since the moments $M^{(i)}(U)$ are exactly the kind of data obtainable with molecular dynamics simulations, the latter may be directly compared with theoretical models. Second, this formulation reveals that full, fitted descriptions of the crater functions are not needed—only the integrated moments show up in the continuum theory. This significantly reduces the number of simulations needed to obtain well-converged data. Last, the use of a formal small parameter ε leads not only to expansions of small quantities (performed previously), but expansions arranged in powers of ε. Because the number of terms associated with increasing powers of ε in the expansion (14) increases rapidly, it is advantageous to show that such terms are formally *small* by powers of ε compared to lower-order terms, so that the series can usually be justifiably truncated at a low order[4].

[4] In certain circumstances, equations truncated at low order in this manner can be ill-posed, when special modes known as *cancelation modes* exhibit nonlinear instability due to cancelation of the limited number of nonlinear terms (see, e.g. [29]). Hence, it can be necessary in those cases to retain even higher-order nonlinearities to regularize the problem. However, in more frequent and less pathologic situations, it is often accurate enough to neglect them. See, for illustration, a comparison between the nonlinear approximation (42) and the full integral equation (23) in [30].

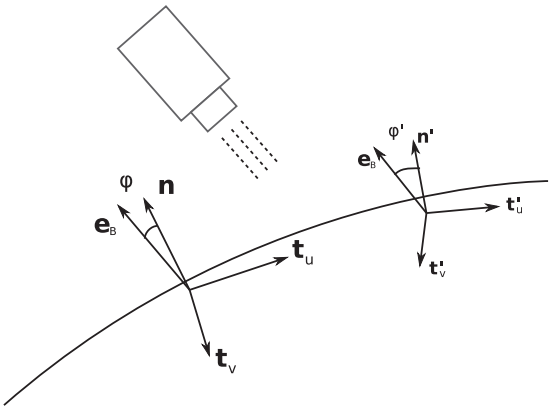

Figure 2. An illustration of the two-dimensional co-ordinate system.

3. Theory—two dimensions

Having covered the essential intuitive concepts of our approach in one dimension, we now briefly extend the theory to two dimensions so that it may be usable in realistic systems. The 1D approach maps step-by-step to the 2D case, except that tensor quantities must now be used instead of scalars.

3.1. Preliminaries

In figure 2 we see a two-dimensional target surface under irradiation, and we again start by defining a *fixed* vector $\mathbf{e}_{\mathrm{B}}$ that points in the direction of the ion source. On this surface, at a point $\mathbf{x}$ of interest, we again define the normal vector $\mathbf{n}$ and the local incidence angle ϕ satisfying $\cos\phi = \mathbf{e}_{\mathrm{B}} \cdot \mathbf{n}$. We then construct a local co-ordinate system about $\mathbf{x}$ using $\mathbf{e}_{\mathrm{B}}$ and the unit normal $\mathbf{n}$. Following [9], we observe that the most natural basis vectors one may use to span the tangent plane are the *downbeam* and *crossbeam* vectors denoted respectively as $\mathbf{t}_u$ and $\mathbf{t}_v$, and given by

$$\begin{aligned} \mathbf{t}_u &= \frac{(-\mathbf{e}_{\mathrm{B}} + (\mathbf{e}_{\mathrm{B}} \cdot \mathbf{n})\,\mathbf{n})}{|-\mathbf{e}_{\mathrm{B}} + (\mathbf{e}_{\mathrm{B}} \cdot \mathbf{n})\,\mathbf{n}|} \\ \mathbf{t}_v &= \mathbf{n} \times \mathbf{t}_u; \end{aligned} \tag{19}$$

i.e., $\mathbf{t}_u$ is just the unit projection of the beam onto the surface, while $\mathbf{t}_v$ is orthogonal to $\mathbf{n}$ and $\mathbf{t}_u$. If we assign co-ordinates $\mathbf{u} = (u, v, w)$ corresponding respectively to the directions $[\mathbf{t}_u, \mathbf{t}_v, \mathbf{n}]$, then surface points $\mathbf{x}'$ in the vicinity of $\mathbf{x}$ can be written

$$\mathbf{x}' = (u, v, h(u, v))\,. \tag{20}$$

This co-ordinate system is natural theoretically because the beam direction vector $\mathbf{e}_{\mathrm{B}}$ is the only fixed object in the system, and so it makes sense to anchor our co-ordinate system to that direction. Additionally, and perhaps more importantly, it is natural for connection with computations because MD simulations are usually performed with a reference direction corresponding to the beam source.

3.2. Basic model

We start our analysis by again imagining an ion impact at some point $\mathbf{x}'$ near to $\mathbf{x}$, and describing the resulting surface response

by the crater function g, which this time is a function of a vector argument $\mathbf{u}'$ rather than a scalar argument u'. In the local co-ordinates about the impact point $\mathbf{x}'$, we write

$$\Delta h(\mathbf{u}') = g\left(\mathbf{u}';\ \mathcal{S}(\mathbf{x}')\right), \tag{21}$$

where $\mathcal{S}$ again indicates a parametric dependence on the surface shape at $\mathbf{x}'$ (local incidence angle, curvatures, etc). From here the continuum description of the normal velocity at $\mathbf{x}$ is again given by integrating the crater function against the flux. As before, to obtain the response at $\mathbf{x}$ to an impact at $\mathbf{x}'$, we must calculate the lateral co-ordinates of $\mathbf{x}$ from the perspective of $\mathbf{x}'$. Thus, we introduce the (vector) quantity $\mathbf{c}(\mathbf{u})$, whose purpose is the same but whose form is somewhat more complicated than the scalar version:

$$\begin{aligned}\mathbf{c}(\mathbf{u}) &= -\begin{bmatrix}\mathbf{t}'_u(\mathbf{u})\cdot(u,v,h)\\ \mathbf{t}'_v(\mathbf{u})\cdot(u,v,h)\end{bmatrix}\\ &= -\left\{\begin{bmatrix}t'_{uu} & t'_{uv}\\ t'_{vu} & t'_{vv}\end{bmatrix}\mathbf{u}+\begin{bmatrix}t'_{uw}\\ t'_{vw}\end{bmatrix}h(\mathbf{u})\right\}\\ &= -\{B(\mathbf{u})\mathbf{u}+\mathbf{b}(\mathbf{u})h(\mathbf{u})\},\end{aligned} \tag{22}$$

where t'_{uv} is the v-component of the tangent $\mathbf{t}_u$, and so on. With this notation, we then immediately write down the integral formula for the normal velocity at $\mathbf{x}$:

$$v_{\mathrm{P}}(\mathbf{x}) = \int R(\mathbf{u})\,\mathrm{d}\mathbf{u} = \int I(\mathbf{u})g\left(\mathbf{c}(\mathbf{u});\ \mathcal{S}(\mathbf{u})\right)\,\mathrm{d}\mathbf{u}, \tag{23}$$

where $R(\mathbf{u})$ is again a notational abbreviation of the integrand. Finally, again, under irradiation with a uniform-intensity beam, the local projected ion flux depends only on the local incidence angle,

$$I(\mathbf{u}) = I_0\mathbf{e}_{\mathrm{B}}\cdot\mathbf{n}(\mathbf{u}) = I_0\cos[\phi(\mathbf{u})]. \tag{24}$$

3.3. Separation of scales

Since the surface is slowly-varying over scales comparable to the size of the impact crater, we again introduce the small parameter ε, and 'small' or 'slow' space variables

$$\mathbf{U} = \begin{bmatrix}U\\ V\\ W\end{bmatrix} = \varepsilon\begin{bmatrix}u\\ v\\ w\end{bmatrix}, \tag{25}$$

so that, again, $\mathbf{U}$ is small in the vicinity of the ion impact. Using this new variable, we explicitly characterize the fast and slow spatial dependencies in the integrand by writing

$$R(\mathbf{u}) = \tilde{R}(\mathbf{u},\mathbf{U}) = \tilde{I}(\mathbf{U})g\left(\tilde{\mathbf{c}}(\mathbf{u},\mathbf{U});\ \tilde{\mathcal{S}}(\mathbf{U})\right), \tag{26}$$

with

$$\begin{aligned}\tilde{I}(\mathbf{U}) &= I(\mathbf{u})\\ \tilde{\mathcal{S}}(\mathbf{U}) &= \mathcal{S}(\mathbf{u})\\ \tilde{B}(\mathbf{U}) &= B(\mathbf{u})\\ \tilde{b}(\mathbf{U}) &= b(\mathbf{u})\\ \tilde{\mathbf{c}}(\mathbf{u},\mathbf{U}) &= -\{\tilde{B}(\mathbf{U})\mathbf{u}+\tilde{\mathbf{b}}(\mathbf{U})h(\mathbf{U})\} = \mathbf{c}(\mathbf{u}).\end{aligned} \tag{27}$$

This again leads directly to a Taylor-series expansion of $\tilde{R}(\mathbf{u},\mathbf{U})$, and we obtain the expression

$$\begin{aligned}R(\mathbf{u}) &= [\tilde{R}]_{\mathbf{U}=0} + \varepsilon\left[\nabla_{\mathbf{U}}\tilde{R}\right]_{\mathbf{U}=0}\cdot\mathbf{u}\\ &\quad+\tfrac{1}{2}\varepsilon^2[\nabla_{\mathbf{U}}\nabla_{\mathbf{U}}\tilde{R}]_{\mathbf{U}=0}\cdot\mathbf{u}\cdot\mathbf{u}+\cdots.\end{aligned} \tag{28}$$

Note that, in two dimensions, the derivatives become gradients, such that $\nabla_{\mathbf{U}}\nabla_{\mathbf{U}}\tilde{R}$ is a rank-two tensor, so that increasing terms of this expansion involve tensors of increasing order. Also note that $\nabla_{\mathbf{U}}$ is just the surface gradient, which is often written $\nabla_{\mathbf{S}}$, a notation we used in section 1 to better serve the casual reader.

3.4. Expression in terms of effective moments

Reaching the stage where we make substitutions, we observe that the $\mathbf{U}$-gradients and $\mathbf{u}$-integrations in (28) can be reversed, and we obtain after some manipulation the form

$$\begin{aligned}v_{\mathrm{P}}(\mathbf{x}) &= \left[(I\tilde{M}^{(0)}) + \varepsilon\nabla_{\mathbf{U}}\cdot(I\tilde{M}^{(1)})\right.\\ &\quad\left.+\tfrac{1}{2}\varepsilon^2\nabla_{\mathbf{U}}\cdot\nabla_{\mathbf{U}}\cdot(I\tilde{M}^{(2)})+\ldots\right]_{\mathbf{U}=0}\end{aligned} \tag{29}$$

(note that gradients became divergences under the reversal of order!), with the effective moments $\tilde{M}^{(i)}$ given by

$$\begin{aligned}\tilde{M}^{(0)} &= \int g\left(\mathbf{c}(\mathbf{u});\mathcal{S}(\mathbf{U})\right)\,\mathrm{d}\mathbf{u}\\ \tilde{M}^{(1)} &= \int g\left(\mathbf{c}(\mathbf{u});\mathcal{S}(\mathbf{U})\right)\,\mathbf{u}\,\mathrm{d}\mathbf{u}\\ \tilde{M}^{(2)} &= \int g\left(\mathbf{c}(\mathbf{u});\mathcal{S}(\mathbf{U})\right)\,\mathbf{u}\otimes\mathbf{u}\,\mathrm{d}\mathbf{u}\\ &\cdots.\end{aligned} \tag{30}$$

Here, the terms $\mathbf{u}$, $\mathbf{u}\otimes\mathbf{u}$, and their followers are now *outer products* of increasing order; i.e.,

$$\mathbf{u} = \begin{bmatrix}u\\ v\end{bmatrix}, \qquad \mathbf{u}\otimes\mathbf{u} = \begin{bmatrix}u^2 & uv\\ uv & v^2\end{bmatrix}, \ldots.$$

3.5. Reduction to actual moments

Our last step is to express the effective moments $\tilde{M}^{(i)}$ in terms of the actual moments $M^{(i)}$:

$$\begin{aligned}M^{(0)}(\mathbf{U}) &= \int g\left(\mathbf{u};\ \mathcal{S}(\mathbf{U})\right)\,\mathrm{d}\mathbf{u}\\ M^{(1)}(\mathbf{U}) &= \int g\left(\mathbf{u};\ \mathcal{S}(\mathbf{U})\right)\mathbf{u}\,\mathrm{d}\mathbf{u}\\ M^{(2)}(\mathbf{U}) &= \int g\left(\mathbf{u};\ \mathcal{S}(\mathbf{U})\right)\mathbf{u}\otimes\mathbf{u}\,\mathrm{d}\mathbf{u}\\ &\cdots.\end{aligned} \tag{31}$$

Again, we do this by introducing into the integrals of (30) a co-ordinate transform, here given by

$$\mathbf{u}\to -\tilde{\mathbf{c}}^{-1}(\mathbf{u},\mathbf{U}) = -\tilde{B}^{-1}(\mathbf{U})\left[\mathbf{u}+h(\mathbf{U})\tilde{\mathbf{b}}(\mathbf{U})\right]. \tag{32}$$

After some simple but tedious calculation, this gives the relations, now using Einstein notation,

$$\begin{aligned}
\tilde{M}^{(0)} &= Q\left[M^{(0)}\right] \\
\tilde{M}^{(1)}_i &= Q\left(-\tilde{B}^{-1}_{ik}\right)\left[M^{(1)}_k + h\tilde{b}_k M^{(0)}\right] \\
\tilde{M}^{(2)}_{ij} &= Q\left(-\tilde{B}^{-1}_{ik}\right)\left(-\tilde{B}^{-1}_{jl}\right) \\
&\quad \times \left[M^{(2)}_{kl} + h\left(\tilde{b}_l M^{(1)}_k + \tilde{b}_k M^{(1)}_l\right) + h^2\tilde{b}_k\tilde{b}_l M^{(0)}\right] \\
&\cdots,
\end{aligned} \tag{33}$$

where

$$Q = \det\left[-\nabla_{\mathbf{u}}\tilde{\mathbf{c}}^{-1}(\mathbf{u},\mathbf{U})\right] = \det[-\tilde{B}^{-1}(\mathbf{U})] = [\det\tilde{B}(\mathbf{U})]^{-1} \tag{34}$$

is the Jacobian of the co-ordinate transformation function. So again, while the mathematics is more complicated in two dimensions, we see that surface evolution depends only on appropriate moments of the crater function $g(\mathbf{u})$. We do note, however, that since the outer products $\mathbf{u}\otimes\mathbf{u}\otimes\cdots$ contain many symmetries, the moments $M^{(i)}$ will also contain them; furthermore, because the statistical surface response to an ion impact should be approximately even in the crossbeam direction v, half of the entries in each tensor $M^{(i)}$ will vanish (namely, those associated with odd powers of v).

4. Example applications

Here we flesh out the actual calculation procedure associated with the methodology of section 3, apply it to some existing theoretical models to demonstrate its agreement, and then develop a method for applying it directly to data from molecular dynamics simulations. Before doing so, however, we wish to make one point on the difference between erosive and redistributive processes. Indeed, the reader will have noticed that the mathematics we have used up to this point has been completely general, depending only on the crater function $g(\mathbf{u})$. However, as has been noted above, this function will naturally describe surface evolution due to two discernible prompt regime mechanisms: (a) mass ejection or sputtering, and (b) local mass redistribution. From the perspective of a generic microscopic picture, neither of these effects ought to be considered as more important than the other. However, because the sputter yield, which has been measured experimentally for many decades, is based on mass ejection and is insensitive to redistribution, the former has been subject to detailed study, while the latter has been more neglected until recently. Thus, one of the aims of this work is to treat both effects with equal rigor. To this end, then, we may simply write

$$g = g_{\text{erosion}} + g_{\text{redist.}}. \tag{35}$$

Expansions based on the former quantity, then, should agree with (or improve upon) existing expansions of Sigmund's ellipse model, while expansions of the second quantity should produce a comprehensive, microscopically-inspired model of the redistributive process. From a modeling perspective, the two components can be treated independently, as we shall see.

4.1. Calculation procedure

Given the moments of the crater function g, we wish to evaluate successive terms of the expansion (29). In addition to the moments, however, a few additional geometric quantities are needed, including $\tilde{B}$, $\tilde{b}$, and trigonometric functions of ϕ. To obtain these, we begin by observing that, at any point $\mathbf{x}$ on the surface, with local incidence angle ϕ_0, we have

$$\mathbf{e}_{\text{B}} = (-\sin\phi_0,\ 0,\ \cos\phi_0)\,. \tag{36}$$

Next, in the vicinity of $\mathbf{x}$, the interface is described by the slowly-varying function

$$W = H(U,V), \tag{37}$$

which allows us to express the normal $\mathbf{n}$ in the usual way as

$$\mathbf{n} = \frac{\left(-\frac{\partial H}{\partial U}, -\frac{\partial H}{\partial V}, 1\right)}{\sqrt{1+\left(\frac{\partial H}{\partial U}\right)^2+\left(\frac{\partial H}{\partial V}\right)^2}}. \tag{38}$$

At this point $\mathbf{t}_u$ and $\mathbf{t}_v$ are given by relations (19), which allows us to construct $\tilde{B}(\mathbf{U})$ and $\tilde{b}(\mathbf{U})$. Finally, trigonometric functions of ϕ, evaluated in the vicinity of $\mathbf{x}$, are obtained using basic vector identities on $\mathbf{e}_{\text{B}}$ (which is constant) and $\mathbf{n}$ (which varies):

$$\begin{aligned}
\cos[\phi(\mathbf{U})] &= \mathbf{e}_{\text{B}}\cdot\mathbf{n} \\
\sin[\phi(\mathbf{U})] &= |\mathbf{e}_{\text{B}}\times\mathbf{n}|\,.
\end{aligned} \tag{39}$$

With all of these quantities, it is now a simple but tedious matter to make the necessary substitutions of moments, matrices, and trigonometric quantities into (29), take the divergences, and evaluate at $\mathbf{U} = 0$. The process may be simplified somewhat if we initially expand $H(U,V)$ as a Taylor expansion in U and V:

$$\begin{aligned}
H(U,V) \approx{}& \tfrac{1}{2}\left(H_{UU}U^2 + 2H_{UV}UV + H_{VV}V^2\right) \\
&+\tfrac{1}{6}(H_{UUU}U^3 + 3H_{UUV}U^2V + 3H_{UVV}UV^2 \\
&+H_{VVV}V^3) + \cdots,
\end{aligned} \tag{40}$$

with all derivatives of H treated as constants evaluated at 0. Then, since we will ultimately be evaluating divergences in (U,V) at zero, it is only necessary throughout the calculation to keep terms in the small U and V up to the order of the moment being evaluated.

4.2. Comparison with existing models

Since our mathematical approach is slightly different than that established in the literature, we first apply our methodology to existing models of erosion and redistribution, showing that one obtains results identical to those already in the literature. In each case, we leave our results in the local co-ordinate system, since this is sufficient for comparison. Conversion to the lab frame is discussed in appendix C.

On the erosive side, we consider Sigmund's ellipsoidal energy-release mechanism. Following [9], we may write down the crater function describing response to the impact of a single

atom in the form

$$g = \frac{(\Lambda\epsilon f)\, a^2}{(2\pi)^{3/2}\,\sigma\,\mu^2}\sqrt{1+H_U^2+H_V^2} \times \exp\left\{-\tfrac{1}{2}a_\mu^2\left[(u\cos\phi + h\sin\phi)^2 + v^2\right] - \tfrac{1}{2}a_\sigma^2\left[u\sin\phi - (1+h\cos\phi)\right]^2\right\}, \tag{41}$$

where the extra factor of $\sqrt{1+H_U^2+H_V^2}$ projects the responses at all nearby points onto the normal at the point of impact. Letting $h(u,v) = \varepsilon^{-1}H(U,V)$ according to equation (25), we obtain the appropriate moments of g (see calculations outlined in appendix B), and then insert these moments into the algebra of section 3 to obtain the result to first order in ε:

$$v_{\mathrm{P}}^{\mathrm{Sig.}} = (I_0/n)Y_0(\phi)\{\cos(\phi) - \varepsilon\left[\Gamma_1(\phi)\,H_{UU} - \Gamma_2(\phi)\,H_{VV}\right]\}, \tag{42}$$

with n, Y_0, Γ_1, Γ_2 defined exactly as in Bradley and Harper [9].

Turning to redistributive effects, a primary motivation of this work, we consider the surface currents due to ballistic atomic drift envisioned in Carter and Vishnyakov (CV) [17]. These authors assume that some proportion α of the lateral component of incoming ion momentum is converted to an atomic surface current $\mathbf{j}$, directed downbeam from the impact point, and having the form

$$\mathbf{j} = \alpha I(\phi)\sin\phi\,\mathbf{t}_u = (\alpha I_0)\cos\phi\sin\phi\,\mathbf{t}_u. \tag{43}$$

Now, we see immediately that this formulation does not constitute a model for the actual surface response. Instead, it is really a theory on the form of the first *moment* of the surface response—indeed, we have simply $M^{(1)}_{\mathrm{redist.}} = \mathbf{j}$. So, to pose the surface current hypothesis within our framework, we ignore the actual crater shape, and simply let:

$$M^{(0)}_{\mathrm{redist.}} = 0 \qquad M^{(1)}_{\mathrm{redist.}} = \begin{bmatrix}\alpha\sin\phi\\ 0\end{bmatrix}, \tag{44}$$

(the zeroth moment is zero by definition, by conservation of mass). Inserting these into the algebra of section 3, the resulting PDE, in two dimensions, is

$$v_{\mathrm{P}}^{\mathrm{CV}} = \varepsilon(\alpha I_0)\left[\cos(2\phi_0)\,H_{UU} + \cos^2(\phi_0)\,H_{VV}\right]. \tag{45}$$

This term agrees with the two-dimensional analysis of the CV mechanism by Davidovitch *et al* [16], after converting to the co-ordinate system used there (CV only studied one dimension). Thus, while our approach is slightly different from preceding approaches in that it deals only with a surface response rather than the underlying models, it returns the same answers when those models are recast in terms of responses or moments.

4.3. Application to molecular dynamics simulations

A general model of redistribution akin to Sigmund's model of erosion would be highly desirable. However, since no such model currently exists, and since ascertaining the accuracy of even Sigmund's model is difficult, there is good reason to consider avoiding models entirely and turning instead directly to direct measurements. Here, while descriptions of $g(\mathbf{u})$ can and have been obtained experimentally [27], in general the separation into erosive and redistributive components requires the use of MD simulation. Thus, we turn our consideration here to the task of obtaining—for both processes—the crater functions and their moments from molecular dynamics simulations. From this perspective, one observes that it is easy to write expression (35), but less obvious how practically to separate the two components of g from a given MD data set. Thus, we here propose a simple technique one could use to do so. Assuming one has available the initial (pre-impact) and final (post-impact) positions of each atom, the first step is to divide the atoms based on whether or not the final location is still attached to the target. If so, the atom is classified as a 'redistributed' atom, while if not, it is classified as a 'sputtered' atom. Then, the assumption of constant density permits one to determine the height change entirely by the lateral components of the displacements of all the atoms. Furthermore, because we actually do not need g itself, but only its moments, we can most effectively obtain the latter by approximating g as an appropriate sum of delta functions over the surface, located at the projected position of each atom.

The erosive component of the crater function, g_{erosive}, is simply the average result of the removal of many single atoms. For the purposes of obtaining moments of this function, we approximate g_{erosive} by placing at the projected initial position $\mathbf{u}_j^{\mathrm{I}} = (u_j^{\mathrm{I}}, v_j^{\mathrm{I}})$ of each sputtered atom j a delta function $\delta(\mathbf{u}_j^{\mathrm{I}})$ of magnitude equal to V_{Si}, the volume of a silicon atom. This gives

$$g_{\mathrm{erosive}}(\mathbf{u}) = -V_{\mathrm{Si}}\sum_j \delta\left(\mathbf{u}_j\right) \tag{46}$$

which, when integrated against the various outer products $\mathbf{u}\otimes\mathbf{u}\ldots$ to obtain the moments (31), will simply pick up point contributions at the initial atomic positions. Thus, if N is the number of sputtered atoms, then the erosive moments $M^{(i)}_{\mathrm{erosive}}$ may be written as sums rather than integrals in the forms

$$M^{(0)}_{\mathrm{erosive}} = -V_{\mathrm{Si}}\sum_{j=1}^{N} 1 \qquad M^{(1)}_{\mathrm{erosive}} = -V_{\mathrm{Si}}\sum_{j=1}^{N}\mathbf{u}_j^{\mathrm{I}} \qquad M^{(2)}_{\mathrm{erosive}} = -V_{\mathrm{Si}}\sum_{j=1}^{N}\mathbf{u}_j^{\mathrm{I}}\otimes\mathbf{u}_j^{\mathrm{I}} \qquad \ldots. \tag{47}$$

For the redistributed atoms k, the process is nearly the same, except that after being moved from a projected initial position $\mathbf{u}_k^{\mathrm{I}}$, the atom resettles at its projected final position $\mathbf{u}_k^{\mathrm{F}}$. So we approximate $g_{\mathrm{redist.}}$ by writing

$$g_{\mathrm{redist.}} = V_{\mathrm{Si}}\sum_k\left[\delta\left(\mathbf{u}_k^{\mathrm{F}}\right) - \delta\left(\mathbf{u}_k^{\mathrm{I}}\right)\right]. \tag{48}$$

Upon integration of (48) over the (u, v) co-ordinate plane, we shall obtain the redistributive moments, also, as sums rather than integrals:

$$\begin{aligned} M^{(0)}_{\text{redist.}} &= 0 \\ M^{(1)}_{\text{redist.}} &= V_{\text{Si}} \sum_{k=1}^{M} \left(\mathbf{u}^{\text{F}}_k - \mathbf{u}^{\text{I}}_k\right) \\ M^{(2)}_{\text{redist.}} &= V_{\text{Si}} \sum_{k=1}^{M} \left(\mathbf{u}^{\text{F}}_k \otimes \mathbf{u}^{\text{F}}_k - \mathbf{u}^{\text{I}}_k \otimes \mathbf{u}^{\text{I}}_k\right) \\ &\cdots \end{aligned} \tag{49}$$

Together, equations (47) and (49) give all the information required.

The approach described here has a number of benefits. First, it avoids the conversion of the atomic displacement set generated by an MD simulation to a height map associated with a continuum surface. For example, one popular method of performing this conversion involves the use of a 'simulated AFM tip' to probe the target and thereby approximate the location of a 'surface.' However, this technique is extremely sensitive to the nature of the tip, and can overestimate the size of hills and underestimate that of valleys; our approach avoids any such errors. Second, as mentioned previously this method implicitly assumes that density is constant throughout the impact process. While this at first might seem a weakness rather than a strength, we argue that, at the fluences required to develop the topographic patterns of interest here, a steady-state density profile must invariably develop on the surface. Hence, densification effects ought similarly to tend to zero over enough properly-designed MD simulations, and so ignoring density variations that do persist may actually hasten convergence. Last, with this method one can easily neglect the contribution of implanted ions to the surface response, which again, over many experiments, must tend to zero anyway.

5. Conclusions

We have introduced a comprehensive framework for coarse-graining the microscopic picture of single ion impact into the prompt regime contribution $v_{\text{P}}(\mathbf{x})$ to a continuum model of surface erosion, based only on the moments of the single-impact crater function. Our framework addresses both erosion and redistribution, and works equally well with theoretical models such as Sigmund's, or moments obtained numerically via MD simulations. The advantages of this approach are fourfold. First and most importantly, writing things in terms of the moments of crater functions explicitly connects the microscopic impact to the macroscopic dynamics, a feature missing until now in treatments of redistribution. Second, it greatly simplifies comparison with molecular dynamics—as we have demonstrated, moments are easy to acquire, and converge after fewer trials than a full description of the crater. Third, a separation of erosive and redistributive components highlights exactly the way these aspects of ion impact compete to determine the macro-scale pattern dynamics. Fourth, while somewhat subtle, the formal use of a small parameter makes clear the relative magnitudes of the multitude of terms which arise from the small curvature expansion. Looking forward, our goal is to apply our methodology to actual molecular dynamics measurements of crater functions so as to obtain a specific prediction—free of tuning parameters—for $v_{\text{P}}(\mathbf{x})$. This, when paired with an appropriate gradual regime contribution $v_{\text{G}}(\mathbf{x})$, will allow direct comparison between the pattern-forming behavior predicted by MD simulations, and that observed in physical experiments performed in the same environmental conditions used in the simulation. This will shed light on the way that crater shape affects continuum predictions, leading to better models of both erosion and redistribution that occur during the impact process.

Acknowledgments

SDG. The authors acknowledge financial support from the following grants: SAN (NSF-DMS0802987), MJA (DE-FG02-06ER46335), MPB (NSF-DMS0605031). We thank Charbel Madi, Kai Nordlund, Juha Samela, Harley Johnson and Naga Kalyanasundaram for helpful discussions.

Appendix A. Estimating the small parameter ε

While the main text of this work focus almost entirely on the prompt regime $v_{\text{P}}(\mathbf{x})$, the small parameter ε is obtained as a ratio of length scales associated with both $v_{\text{P}}(\mathbf{x})$ and $v_{\text{G}}(\mathbf{x})$. In the prompt regime, erosion due to ion impacts can be described by the equation

$$v_{\text{P}}(\mathbf{x}) = v_0 \times G(\mathcal{S}), \tag{50}$$

where v_0 is a characteristic surface erosion velocity, and $G(\mathcal{S})$ is a non-dimensionalized function containing the (integrated) geometry dependence of the problem. In contrast, in the gradual regime, one may consider ion-enhanced surface viscous flow [20], which is modeled by the equation

$$v_{\text{G}}(\mathbf{x}) = -\frac{\gamma \Omega^3}{3\eta} \times \nabla^2_{\mathbf{S}} \mathcal{K}, \tag{51}$$

where γ is the surface energy, d the viscous-layer depth, η the viscous-layer viscosity, and $\nabla^2_{\mathbf{S}}\mathcal{K}$ is the surface Laplacian of the mean curvature. For a theory including both processes (e.g. [31, 32]), the 'surface-diffusion-like' coefficient $\gamma a^3/\eta$ may be balanced with the driving erosion velocity $\Lambda \epsilon f$ to obtain a characteristic macroscopic length scale L, satisfying

$$L = d \left(\frac{\gamma}{v_0 \eta}\right)^{1/3}. \tag{52}$$

Upon comparing this with a *microscopic* length scale given by the penetration depth $a \approx d$, we find that ε, the ratio of micro- to macro-scales, is estimated to be

$$\varepsilon = \left(\frac{v_0 \eta}{\gamma}\right)^{1/3}. \tag{53}$$

Under what conditions is this, in fact, small? A model for the scaling of the characteristic velocity (loosely following [9]) is

$v_0 = LEF$, where F is the flux of ions through a plane normal to the ion beam source, E is the energy per incident ion, and L a proportionality constant relating the erosion velocity to the power deposition. Looking over the components of ε, we observe that γ is a material constant, while c is also essentially constant, depending only on the irradiating and target atoms over a wide range of ion energies. Finally, the viscosity η scales inversely with the flux over a wide range of fluxes. Hence, the only parameter left in ε is the energy E, and so we expect ε to be small in the low-energy limit.

Appendix B. Sigmund moment calculations

We begin by writing the Sigmund response (41) in the compact form

$$g = \gamma \mathrm{e}^{-[\alpha y^2 + \beta(x-\delta)^2]} \tag{54}$$

where, after letting $h = \varepsilon^{-1} H(U, V)$, we follow the conventions in Bradely and Harper [9] to obtain

$$\begin{aligned}
\alpha &= \tfrac{1}{2} a_\mu^2 \\
\beta &= \tfrac{1}{2} B_1 \\
\delta(H) &= \frac{\left(A - 2C\frac{H}{\varepsilon}\right)}{B_1} \\
\gamma(H) &= \frac{(\Lambda \epsilon f)\left(a_\sigma a_\mu^2\right)}{(2\pi)^{3/2}} \sqrt{1 + H_U^2 + H_V^2} \\
&\times \exp\left\{ -\frac{1}{2}\left[a_\sigma^2 + 2B_2 \frac{H}{\varepsilon} + 8D\left(\frac{H}{\varepsilon}\right)^2 \right.\right. \\
&\left.\left. - \frac{\left(A - 2C\frac{H}{\varepsilon}\right)^2}{B_1} \right] \right\},
\end{aligned} \tag{55}$$

where

$$\begin{aligned}
A(\phi) &= a_\sigma^2 \sin\phi \\
B_1(\phi) &= a_\sigma^2 \sin^2\phi + a_\mu^2 \cos^2\phi \\
B_2(\phi) &= a_\sigma^2 \cos\phi \\
C(\phi) &= \tfrac{1}{2}\left(a_\mu^2 - a_\sigma^2\right) \sin\phi \cos\phi \\
D(\phi) &= \tfrac{1}{8}\left(a_\mu^2 \sin^2\phi + a_\sigma^2 \cos^2\phi\right).
\end{aligned} \tag{56}$$

From the form (54), the first few moments are then easily calculated, with

$$\begin{aligned}
M^0 &= \gamma(H) \sqrt{\frac{\pi^2}{\alpha\beta}} \\
M_x^1 &= M^0(\delta) \\
M_{xx}^2 &= M^0\left(\frac{1}{2\beta} + \delta^2\right) \\
M_{yy}^2 &= M^0\left(\frac{1}{2\alpha}\right).
\end{aligned} \tag{57}$$

These moments are then used for the calculations in the main text.

Appendix C. Conversion to lab co-ordinates

In the main text, results were presented in the local co-ordinate system for consistency and brevity. However, for linear, weakly-nonlinear, or fully-geometric investigation, it is obviously desirable to express equations in the global co-ordinate system. This, however, is simply a straightforward (if tedious) geometric exercise. A discussion of the process in the context of sputtering is available in [13]; here, we simply repeat the essential points.

To convert to the lab frame, we simply need to express the normal, tangents, and local beam intensity I in terms of lab-accessible quantities, namely θ, h_x, and h_y. We already saw that $I = I_0 \mathbf{e}_\mathrm{B} \cdot \mathbf{n}$, and some further algebra reveals that

$$T = [\mathbf{t}_u, \mathbf{t}_v, \mathbf{n}] = \begin{bmatrix} \frac{\left(1+h_y^2\right)\sin\theta - h_x\cos\theta}{g\sin\phi} & \frac{h_y\cos\theta}{\sqrt{g}\sin\phi} & \frac{-h_x}{\sqrt{g}} \\ \frac{-h_x h_y\sin\theta - h_y\cos\theta}{g\sin\phi} & \frac{\sin\theta - h_x\cos\theta}{\sqrt{g}\sin\phi} & \frac{-h_y}{\sqrt{g}} \\ \frac{h_x\sin\theta - \left(h_x^2+h_y^2\right)\cos\theta}{g\sin\phi} & \frac{h_y\sin\theta}{\sqrt{g}\sin\phi} & \frac{1}{\sqrt{g}} \end{bmatrix}, \tag{58}$$

where

$$\begin{aligned}
g &= h_x^2 + h_y^2 + 1 \\
\cos\phi &= \left(h_x \sin\theta + \cos\theta\right)/\sqrt{g} \\
\sin\phi &= \left[(\sin\theta - h_x\cos\theta)^2 + h_y^2\right]^{1/2}/\sqrt{g}.
\end{aligned} \tag{59}$$

With this information, the divergence operators are converted from the local frame to the lab frame via

$$\nabla_\mathbf{U} = \frac{\partial}{\partial U_i} = \frac{\partial x_j}{\partial U_i}\frac{\partial}{\partial x_j} = \tilde{B}^T \nabla_\mathbf{x}. \tag{60}$$

Note that, for surface divergences, since we are only interested in the tangential directions, we only use the upper-left 2×2 block of T, which is here denoted $\tilde{B}$ as in the main text.

References

[1] Navez M, Chaperot D and Sella C 1962 Microscopie electronique—etude de lattaque du verre par bombardement ionique *C. R. Hebd. Seances Acad. Sci.* **254** 240

[2] Chan W L and Chason E 2007 Making waves: kinetic processes controlling surface evolution during low energy ion sputtering *J. Appl. Phys.* **101** 121301

[3] Wei Q, Lian J, Zhu S, Li W, Sun K and Wang L 2008 Ordered nanocrystals on argon ion sputtered polymer film *Chem. Phys. Lett.* **452** 124

[4] Cuenat A, George H B, Chang K-C, Blakely J M and Aziz M J 2005 Lateral templating for guided self-organization of sputter morphologies *Adv. Mater.* **17** 2845

[5] Yamada I, Matsuo J, Toyoda N and Kirkpatrick A 2001 Materials processing by gas cluster ion beams *Mater. Sci. Eng.* R **34** 231

[6] Adams D P, Aziz M J, Hobler G, MoberlyChan W J and Schenkel T 2007 Fundamentals of FIB nanostructural processing: below, at and above the surface *MRS Bull.* **32** 424

[7] Sigmund P 1969 Theory of sputtering. I. Sputtering yield of amorphous and polycrystalline targets *Phys. Rev.* **184** 383–416

[8] Sigmund P 1973 A mechanism of surface micro-roughening by ion bombardment *J. Mater. Sci.* **8** 1545–53

[9] Bradley R M and Harper J M E 1988 Theory of ripple topography induced by ion bombardment *J. Vac. Sci. Technol.* **6** 2390–5
[10] Herring C 1950 Effect of change of scale on sintering phenomena *J. Appl. Phys.* **21** 301
[11] Mullins W W 1959 Flattening of a nearly plane solid surface due to capillarity *J. Appl. Phys.* **30** 77
[12] Makeev M A and Barabási A-L 1997 Ion-induced effective surface diffusion in ion sputtering *Appl. Phys. Lett.* **71** 2800–2
[13] Makeev M A, Cuerno R and Barabási A-L 2002 Morphology of ion-sputtered surfaces *Nucl. Instrum. Methods Phys. Res.* B **197** 185–227
[14] Kim T C, Ghim C-M, Kim H J, Kim D H, Noh D Y, Kim N D, Chung J W, Yang J S, Chang Y J, Noh T W, Kahng B and Kim J-S 2004 Kinetic roughening of ion-sputtered Pd(001) surface: beyond the Kuramoto–Sivashinsky model *Phy. Rev. Lett.* **92** 246104
[15] Feix M, Hartmann A K and Kree R 2005 Influence of collision cascade statistics on pattern formation of ion-sputtered surfaces *Phys. Rev.* B **71** 125407
[16] Davidovitch B, Aziz M J and Brenner M P 2007 On the stabilization of ion sputtered surfaces *Phys. Rev.* B **76** 205420
[17] Carter G and Vishnyakov V 1996 Roughening and ripple instabilities on ion-bombarded Si *Phys. Rev.* B **54** 17647–53
[18] Moseler M, Gumbsch P, Casiraghi C, Ferrari A C and Robertson J 2005 The ultrasmoothness of diamond-like carbon surfaces *Science* **309** 1545–8
[19] Castro M, Cuerno R, Vásquez L and Gago R 2005 Self-organized ordering of nanostructures produced by ion-beam sputtering *Phys. Rev. Lett.* **94** 016102
[20] Umbach C C, Headrick R L and Chang K-C 2001 Spontaneous nanoscale corrugation of ion-eroded SiO_2: the role of ion-irradiation-enhanced viscous flow *Phys. Rev. Lett.* **87** 246104
[21] Alkemade P F A 2006 Propulsion of ripples on glass by ion bombardment *Phys. Rev. Lett.* **96** 107602
[22] Facsko S, Bobek T, Stahl A and Kurz H 2004 Dissipative continuum model for self-organized pattern formation during ion-beam erosion *Phys. Rev.* B **69** 153412
[23] Vogel S and Linz S J 2006 How ripples turn into dots: modeling ion-beam erosion under oblique incidence *Europhys. Lett.* **76** 884–90
[24] Bringa E M, Nordlund K and Keinonen J 2001 Cratering energy regimes: from linear collision cascades to heat spikes to macroscopic impacts *Phys. Rev.* B **64** 235426
[25] Kalyanasundaram N, Ghazisaeidi M, Freund J B and Johnson H T 2008 Single impact crater functions for ion bombardment of silicon *Appl. Phys. Lett.* **92** 131909
[26] Aste T and Valbusa U 2004 Surface instabilities in granular matter and ion-sputtered surfaces *Physica* A **332** 548–58
[27] Costantini G, Buatier de Mongeot F, Boragno C and Valbusa U 2001 Is ion sputtering always a 'negative homoepitaxial deposition'? *Phys. Rev. Lett.* **86** 838
[28] Aziz M J 2006 Nanoscale morphology control using ion beams *Matematisk-fysiske Meddelelser* **52** 187
[29] Muñoz-García J, Castro M and Cuerno R 2006 Nonlinear ripple dynamics on amorphous surfaces patterned by ion beam sputtering *Phys. Rev. Lett.* **96** 086101
[30] Chen H H, Urquidez O A, Ichim S, Rodriquez L H, Brenner M P and Aziz M J 2005 Shocks in ion sputtering sharpen steep surface features *Science* **310** 294–7
[31] Vauth S and Mayr S G 2007 Relevance of surface viscous flow, surface diffusion, and ballistic effects in keV ion smoothing of amorphous surfaces *Phys. Rev.* B **75** 224107
[32] Vauth S and Mayr S G 2008 Ion bombardment induced smoothing of amorphous metallic surfaces: experiments versus computer simulations *Phys. Rev.* B **77** 155406